#### **PAPER**

# Optimization of 3D printing parameters for ${\rm BaTiO_3}$ piezoelectric ceramics through design of experiments

To cite this article: Anabel Renteria et al 2019 Mater. Res. Express 6 085706

View the article online for updates and enhancements.

#### Recent citations

- <u>Electromechanical Properties of</u> <u>Robocasted Barium Titanate Ceramics</u> <u>Mylena Lorenz *et al*</u>
- Particle size influence on material properties of BaTiO<sub>3</sub> ceramics fabricated using freeze-form extrusion 3D printing Anabel Renteria et al



### IOP ebooks™

Bringing together innovative digital publishing with leading authors from the global scientific community.

Start exploring the collection-download the first chapter of every title for free.

#### Materials Research Express



RECEIVED 8 April 2019

REVISED

25 April 2019

ACCEPTED FOR PUBLICATION 8 May 2019

PUBLISHED 24 May 2019

#### **PAPER**

## Optimization of 3D printing parameters for $BaTiO_3$ piezoelectric ceramics through design of experiments

Anabel Renteria o, Hilda Fontes, Jorge A Diaz, Jaime E Regis, Luis A Chavez o, Tzu-Liang (Bill) Tseng, Yingtao Liu o and Yirong Lin

- 1 Department of Mechanical Engineering, University of Texas at El Paso, El Paso 79968, United States of America
- Department of Industrial, Manufacturing, and Systems Engineering, University of Texas at El Paso, El Paso 79968, United States of America
- 3 Department of Aerospace and Mechanical Engineering, The University of Oklahoma, Norman, OK, 73019, United States of America

E-mail: arenteriamarquez@miners.utep.edu

Keywords: additive manufacturing, piezoelectric, design of experiments

Supplementary material for this article is available online

#### **Abstract**

Paste extrusion is an additive manufacturing technique that deposits paste through a nozzle in a layer-by-layer fashion to form a three-dimensional object. This technique can be used to fabricate piezoelectric ceramics with complex geometries and excellent material properties to fabricate sensors, capacitors, and energy storage devices with a high level of customization. Different factors can affect the quality of piezoelectric ceramics when using the paste extrusion technique, for example, the composition of the paste and printing parameters. This paper presents a study to optimize the piezoelectric coefficient, relative density, dielectric permittivity and dimensional accuracy of BaTiO<sub>3</sub> by using design of experiments with a 2<sup>k-1</sup> design. Results indicated that the factors having a significant impact on the end-product outputs were the BaTiO<sub>3</sub> particle size and the binder concentration on the paste formulation. Using the optimal levels makes it possible to achieve a piezoelectric coefficient higher than 200 pC/N and a density of 90% of the theoretical value of pure BaTiO<sub>3</sub>.

#### 1. Introduction

Additive Manufacturing (a.k.a. 3D Printing) consists of the deposition of material in a layer-by-layer fashion to form a three-dimensional object. This technique is widely used for rapid prototyping, especially when the fabrication of complex geometries is required. Materials including metals, polymers, and ceramics are used for additive manufacturing processes [1]. Literature reports efforts in the fabrication of ceramics using different additive manufacturing techniques such as material jetting, material extrusion, direct energy deposition, binder jetting and stereolithography [2, 3]. The fabrication of ceramics is an area of interest due to their excellent thermal, mechanical, and electric properties, which are useful in several applications in the area of electronics and beyond [4, 5]. However, ceramics fabricated using additive manufacturing are hard to process because they must be sintered to remove the binder content to obtain a densified sample [3]. This debinding process can lead to nonconforming samples with high levels of porosity especially for powder-based methods, or inhomogeneity causing cracks and reducing the mechanical strength of the final product for slurry-based methods [6]. For this reason, the fabrication of ceramics with designed complex geometries and defects-free becomes a challenge.

Many research studies have been reported on the fabrication of technical or functional ceramic objects using free-forming techniques. Freeze-form Extrusion Fabrication (FEF), Ceramic Extrusion On Demand (CODE) and Robocasting are some examples of this technique [7]. For technical ceramics, researches commonly reported the use of Alumina  $(Al_2O_3)$  [3, 8, 9], Silica  $(SiO_2)$  [10] and Silicon Nitrate  $(Si_3N_4)$  [11]. For example, Huang *et al* used FEF to fabricate complex geometries with  $Al_2O_3$  achieving a density of 90% with respect to the theoretical value [9]. For functional ceramics, researchers reported studies using ferroelectric ceramics [12] and magnetic ferrite ceramics [13, 14]. Ferroelectric ceramics are specifically of interest due to their piezoelectric

properties. Piezoelectricity refers to the generations of an electric signal when mechanical loads are applied or vice versa [15]. Pb( $Zr_xTi_{1-x}$ )O<sub>3</sub> or PZT is a ferroelectric ceramic known to have good piezoelectric properties ( $d_{33}\sim500-600$  pC/N) [16], and it is widely used for sensors and capacitors applications [17]. However, the use of toxic materials such as lead oxide (PbO), especially for electronic devices could increase the environmental pollution and harm the human body [18–21]. Many efforts have been focused on lead-free ferroelectric ceramics, such as KNN, BT, BNT based ceramics [19, 20]. Barium Titanate (BaTiO<sub>3</sub> or BTO), is known to have good piezoelectric properties ( $d_{33}\sim190$  pC/N) [21] and can be used as sensors and capacitors with comparable properties to PZT.

Although Additive Manufacturing enables the fabrication of ceramics with complicated design, the optimization of the fabrication process is still required. Design of Experiments (DOE) is a statistical tool that evaluates different factors and their impact in the end-product output. DOE also allows to determine the optimal level of these factors to maximize the desired output. Several authors have used statistical analysis to optimize the fabrication process for different additive manufacturing techniques [22–25]. For example, Chen and Zhao investigated the process parameters that influence the surface quality of stainless steel powder manufactured with Binder Jetting technique using Signal to Noise ratio and ANOVA analysis. The factors considered in this study were layer thickness, printing saturation, heater powder ratio and drying time. They demonstrated that layer thickness was the most significant factor affecting surface roughness. The drying process showed the highest impact on the shrinkage of the samples [22]. Yan *et al* investigated the factors that affect the liquid phase migration of Al<sub>2</sub>O<sub>3</sub> fabricated with FEF. The factors studied were extrusion velocity, extrusion interval time and nozzle length and analyzed with an orthogonal design of experiments. It was found that extrusion velocity and extrusion interval time have an impact on the liquid phase migration of FEF [25].

Even though a considerable amount of research has been dedicated to the optimization of ceramics, there is insufficient work reported on functional ceramics such as piezoelectrics. To obtain high-quality ceramics, techniques such as FEF have been developed to increase density and piezoelectric properties. FEF is an additive manufacturing technique that extrudes and deposits paste through a nozzle onto a substrate below the freezing temperature of the paste. This free-forming technique is an inexpensive slurry-based method that can fabricate complex designs of ceramics with better shape retention and high density. This paper aims to optimize the fabrication of BaTiO $_3$  ferroelectric ceramics using FEF technique through DOE with a fractional factorial  $2^{k-1}$  design. This study considers the evaluation of four different factors: particle size, binder amount, nozzle diameter, and printing speed.

#### 2. Experimental details

#### 2.1. Materials and paste preparation

BaTiO<sub>3</sub> powder supplied from Inframat (Manchester, CT) was selected as solid loading of the paste. Polyvinyl Alcohol (PVA) powder (Mw~89,000–98,000) supplied from Sigma Aldrich (St. Louis, MO) was determined to be the binder in the ceramic suspensions. For the paste preparation, PVA powder was dissolved in deionized water using a stirring rate of 500 rpm and let to dwell for 20 min. Then, the solution was placed in a hot plate at 90 °C for 20 min to achieve a homogeneous dispersion of the PVA powder. After that, BaTiO<sub>3</sub> powder was added to the solution and mixed until a homogenous paste was obtained. All the ceramics suspensions were fabricated using 70 wt% BaTiO<sub>3</sub> and 30 wt% PVA solution. Lastly, the paste was deposited into a syringe tube and sealed immediately to prevent water evaporation.

#### 2.2. Factors and levels

A two-level fractional factorial design  $2^{k-1}$  was selected to optimize the fabrication of BaTiO<sub>3</sub> ferroelectric ceramics. This statistical design considers the evaluation of k factors with two levels of interest. However, when a large number of factors are evaluated, it is recommended that a k-1 design is used, as the number of runs per replications could overcome available resources [26]. Table 1 refers to the factors and levels considered for this study. BaTiO<sub>3</sub> particle size was selected as a factor, using 300 nm as high level and 100 nm as low level. The particle size of BaTiO<sub>3</sub> is a factor of interest as it may influence the mechanical properties of the final product [27]. The PVA concentration was also selected, since the binder content may affect the rheology of the ceramic suspensions [28]. The high level of PVA was set to 13 wt% in deionized water, and the low level was set to 9 wt% in deionized water. Another factor was printing speed; since different flow-rates can affect the relative density and the dimensional accuracy of the green bodies [29]. The high and low level for printing speed was set to 20 mm s<sup>-1</sup> and 10 mm s<sup>-1</sup> respectively. The last factor selected was the nozzle diameter; the high level was set to 1.2 mm while the low level was set to 0.8 mm. The nozzle diameter can possibly affect the dimensional accuracy of the green bodies due to the shear stress generated in the walls of the nozzle and the stress required for the piston of the machine to achieve a constant flow [30]. The fractional factorial design  $2^{k-1}$  was created with

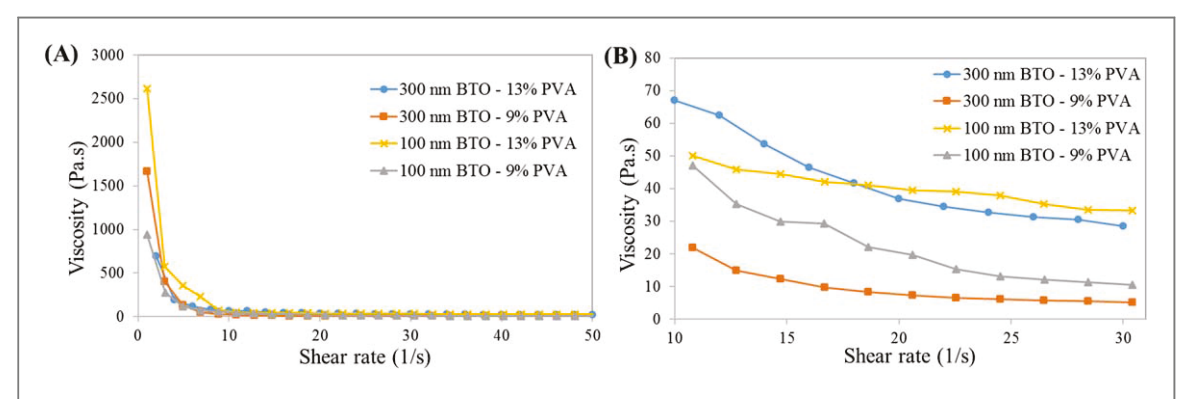


**Figure 1.** Viscosity profile as a function of shear rate for each BTO-PVA ceramic suspension (A) shear rate in the ranges of 1 to  $50 \, \text{s}^{-1}$  (B) Magnification of viscosity in a shear rate range of  $10 \, \text{to} \, 30 \, \text{s}^{-1}$ .

**Table 1.** Factors and levels for design of experiments.

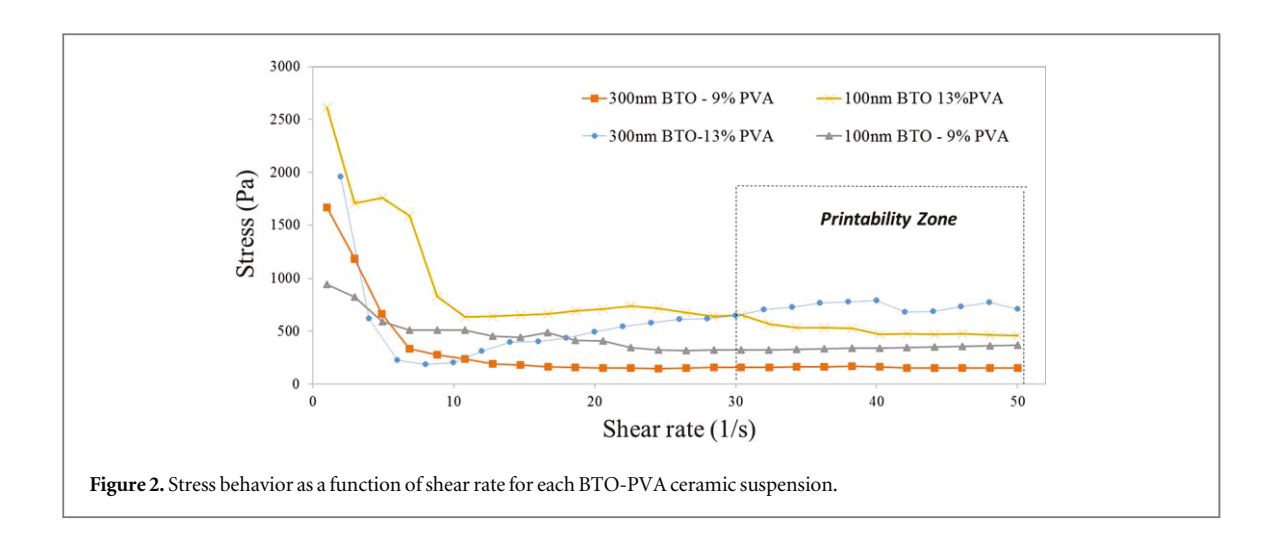
|                        | Levels                 |                        |  |
|------------------------|------------------------|------------------------|--|
| Factors                | Low                    | High                   |  |
| PVA in deionized water | 9 wt%                  | 13 wt%                 |  |
| BTO particle size      | 100 nm                 | 300 nm                 |  |
| Printing speed         | $10\mathrm{mm~s}^{-1}$ | $20\mathrm{mm~s}^{-1}$ |  |
| Nozzle diameter        | 0.8 mm                 | 1.2 mm                 |  |

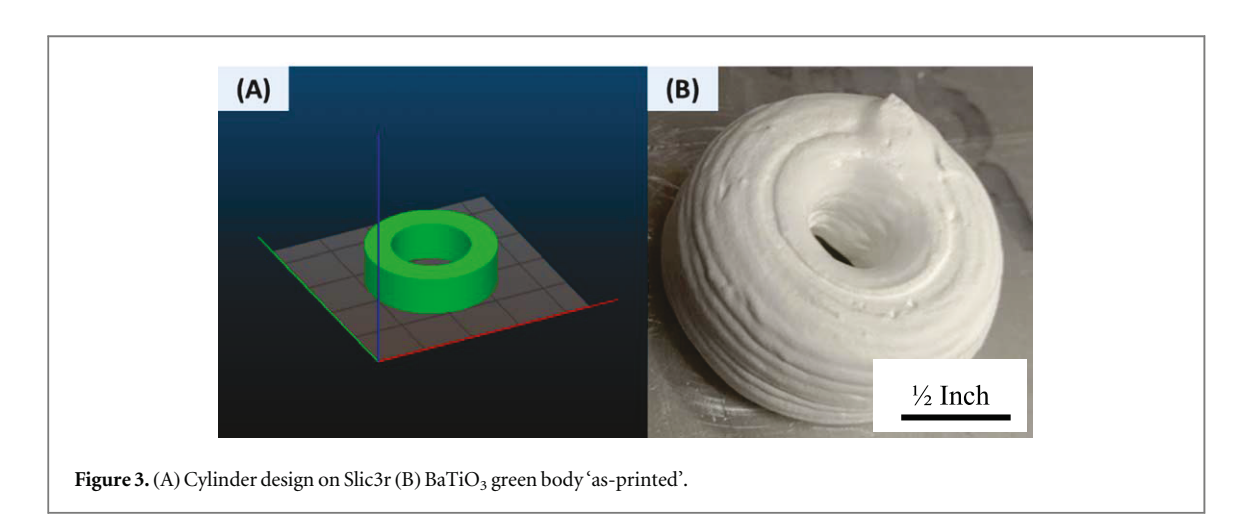
Table 2. Runs per replication.

| Run | PVA in<br>deionized<br>water (wt%) | BTO<br>particle<br>size (nm) | Printing<br>speed<br>(mm s <sup>-1</sup> ) | Nozzle<br>diameter<br>(mm) |
|-----|------------------------------------|------------------------------|--|----------------------------|
| 1   | 9                                  | 100                          | 10   | 0.8                        |
| 2   | 9                                  | 100                          | 20   | 1.6                        |
| 3   | 9                                  | 300                          | 20   | 0.8                        |
| 4   | 9                                  | 300                          | 10   | 1.6                        |
| 5   | 13                                 | 100                          | 20   | 0.8                        |
| 6   | 13                                 | 100                          | 10   | 1.6                        |
| 7   | 13                                 | 300                          | 10   | 0.8                        |
| 8   | 13                                 | 300                          | 20   | 1.6                        |

Minitab using the information provided in table 1. This study considers three replications and a randomized order to validate the results. Table 2 shows an example of the runs required, considering all the different runs for one replication.

The factors and levels selected in table 1 are justified with the rheology characterization of the paste formulation. Proper rheology can guarantee a constant flow and printability of the samples [30]. All the different pastes were measured in a DHR-2 rheometer (TA Instruments, New Castle, DE) at room temperature, using a parallel geometry with a 1.2 mm gap. Figure 1(A) shows the viscosity of each ceramic suspension as a function of shear rate in the ranges of 1 to 50 s<sup>-1</sup>; while figure 1(B) shows a magnified version of the viscosity in a shear rate of 10 to 30 s<sup>-1</sup>. Figure 2 shows the stress profile at different shear rates in the ranges of 1 to 50 s<sup>-1</sup>. All the ceramic suspensions presented a shear thinning behavior [30, 31] as low shear rates require higher force due to the initial viscosity of the paste. However, high shear rates require lower applied force. The initial high force is required to generate the flow through the nozzle. Also known as the dynamic yield stress of the fluid [30]. It was found that the suspensions with higher PVA concentration had a higher viscosity and thus required more initial force applied. Furthermore, it was observed that finer particle size of BaTiO<sub>3</sub> also affects the viscosity. The rheology of the different ceramic suspensions is in good agreement with literature according to the following. PVA behaves as a non-Newtonian fluid in aqueous solutions and exhibits different viscoelastic properties depending on the concentration [30]. The increment on the viscoelastic properties observed can be attribute to a stronger hydrogen-bonding interaction of PVA when increasing its content [30]. Literature suggest that particle size also





affects the rheology of the suspensions. Finer size could increase the contact between particles dispersed in the suspension affecting the viscosity [31]. The increase in viscosity can be attributed to liquid trapped inside aggregates of powder within the paste [32]. Figure 2 shows the printability zone at shear rates of 30 to  $50 \, \mathrm{s}^{-1}$  with ranges in viscosity between 40 to 10 Pa.s. Different viscosity values will affect the flow rate of the suspension during the fabrication of the samples and needs to be evaluated.

#### 2.3. Fabrication process

The samples were printed using a Printrbot Simple Metal 3D printing machine, which was modified to extrude paste. A cylinder of 1-inch outer diameter, 1/2-inch inner diameter, and 1/2-inch height was selected as the standard sample for this study. Figure 3(A) shows the CAD design of the cylinder in Slic3r software. The printing process of the samples follows a randomized order. Additionally, the samples were identified immediately with the run number according to the DOE table (supplementary section 1-figure 9 is available online at stacks.iop. org/MRX/6/085706/mmedia). During the printing, an aluminum freezing plate was placed onto the substrate at -40 °C. The plate was covered with a thin film to allow for an easier detachment of the samples. After printing, the aluminum plate was removed from the bed and placed in a freezer at -60 °C (Thermo Scientific  $TSU^{TM}$  Series  $-86\,^{\circ}$ C Upright Ultra-Low) for 12 h to dry some of the water content by sublimation. To prevent the generation of cracks, the samples were placed upside down in the freezer for another 30 min. The samples were also dried in an electric oven (Lab companion OF-01E) at 40 °C for 24 h to remove any remaining water from the green body. A slow drying process under low temperatures prevents the generation of microcracks in the green bodies [33]. Figure 3(B) shows an example of an as-printed BaTiO<sub>3</sub> sample. The angle after drying was measured, comparing the displacement of the last printed layer with respect to the first layer (supplementary section 2-figure 10). Some of the samples presented an inferior ability to stack the material during the printing process. This issue was observed mainly on the pastes that contained a higher water content level. The density of the green bodies was measured using Archimedes' principle and compared with the theoretical density of

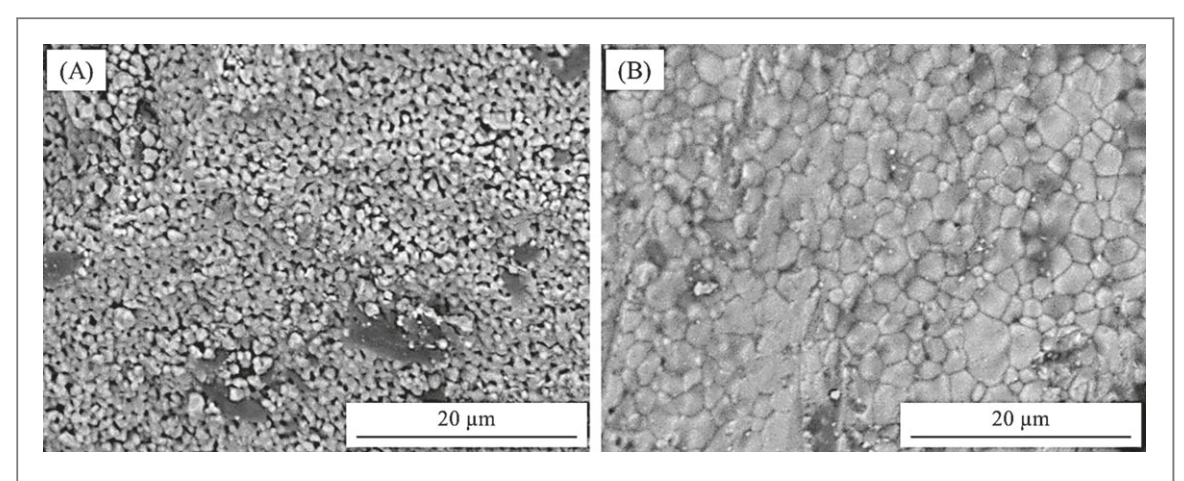
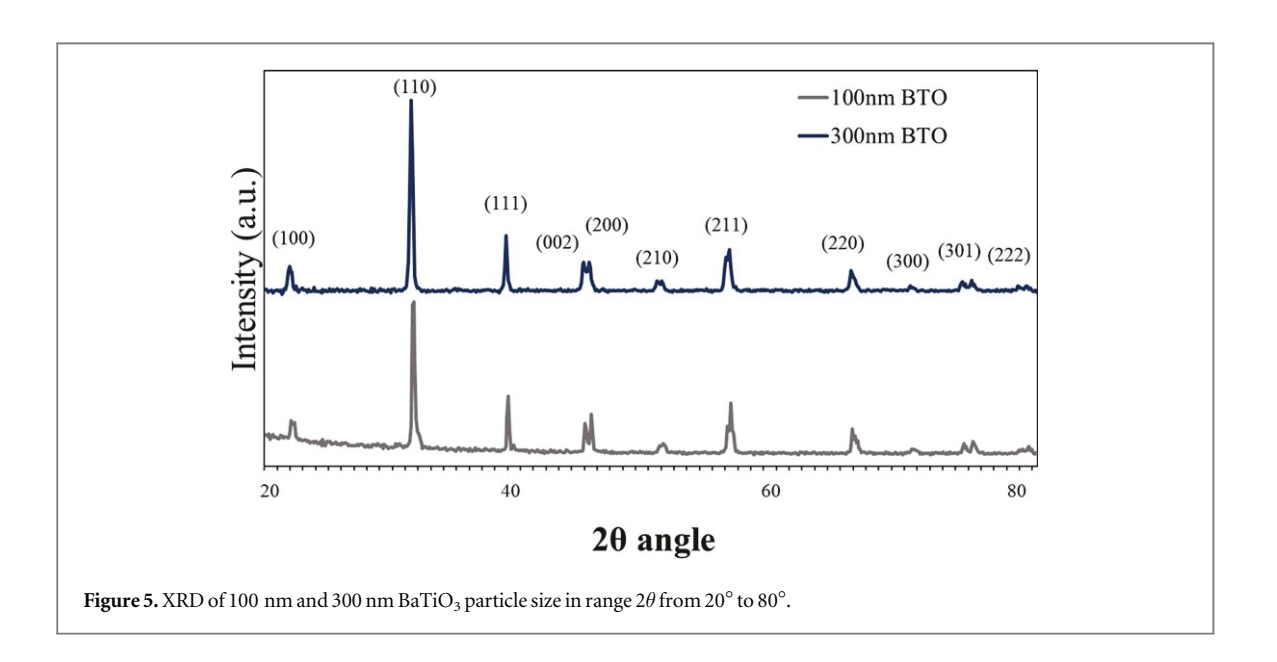


Figure 4. (A) Cross section of a 300 nm BaTiO<sub>3</sub> 9 wt% PVA sample after sintering (B) Cross section of a 100 nm BaTiO<sub>3</sub> 13 wt% PVA sample after sintering.



 $BaTiO_3$  of 6.02 g cm<sup>-3</sup> [34] (supplementary section 3-table 3). The density of the green bodies was 1.67 g cm<sup>-3</sup> on average before sintering. This relatively low-density value is attributed to the amount of water and binder content in the as-printed samples.

#### 2.3.1. Post-processing and material characterization

All the samples were debinded at 600 °C for one hour and sintered at 1250 °C for two hours at 5 °C min<sup>-1</sup> ramp. After sintering, the samples were polished using sandpaper 240-grit. Conductive silver paint was applied in the top surface, then dried at 400 °C for 15 min. The same process was repeated for the bottom surface of the samples. Each sample was exposed to thermal poling on silicon oil for 2 h for dipoles alignment. The electrical field and the temperature were set to 5.4 kV cm<sup>-1</sup> and 90 °C respectively [35]. The piezoelectric coefficient was calculated using a  $d_{33}$  meter (APC YE2730A). Dielectric permittivity was calculated with an LCR meter (1920 Precision, IET lab).

The grain morphology characterization of the samples after sintering was observed using a scanning electron microscope (SEM, TM-1000 Hitachi). Figure 4(A) shows the cross-section of a 300 nm BaTiO<sub>3</sub> and 9% PVA sample after sintering. The density for this sample was 4.03 g cm<sup>-3</sup>, which represents 66.95% of the theoretical value. It was also observed that the grain size was  $\emptyset \simeq 0.9 \ \mu \text{m}$  on average. Figure 4(B) presents the cross-section of a 100 nm BaTiO<sub>3</sub> and 13% PVA sample after sintering. The density for this sample was 5.22 g cm<sup>-3</sup>, which represents 86.75% of the theoretical value. The 100 nm BaTiO<sub>3</sub> sample showed bigger grain sizes of  $\emptyset \simeq 1.8 \ \mu \text{m}$  on average. There is an evident increase in density for finer particle sizes. Researchers suggest that finer particle size tends to achieve a higher grain growth due to high curvature of the ceramic powder, which requires a lower change in energy during sintering [36].

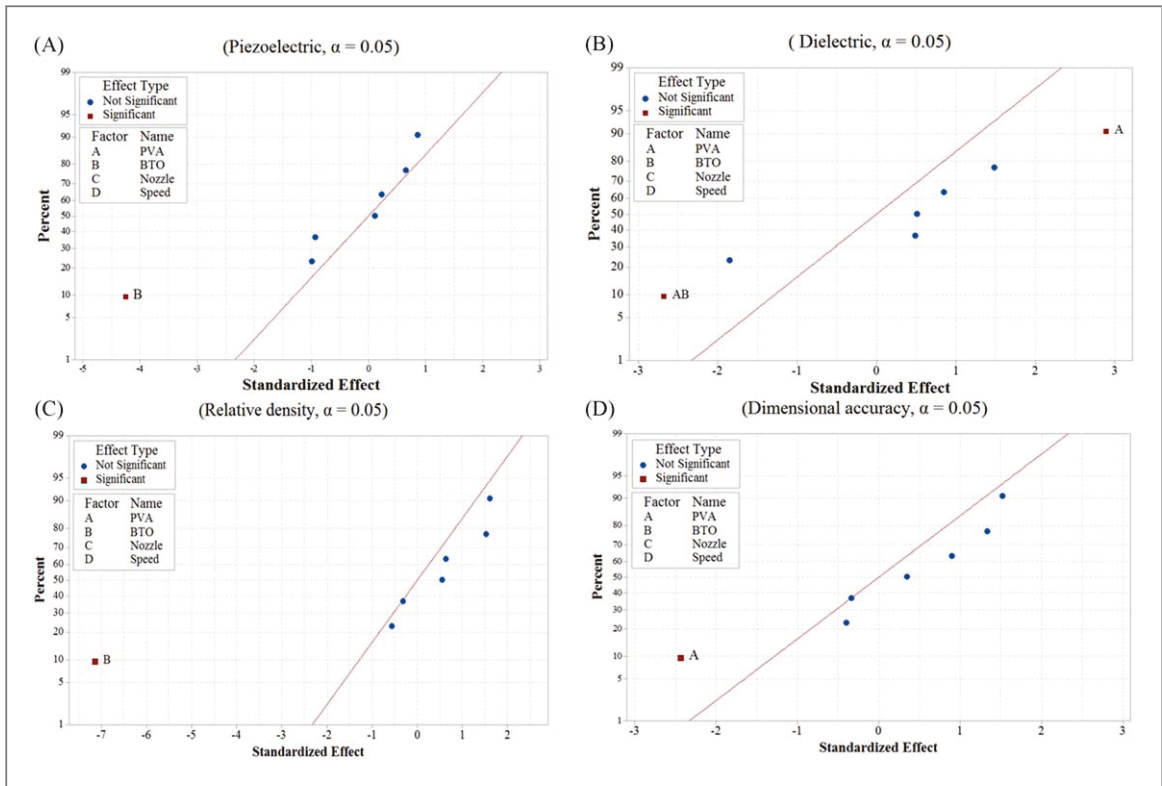


Figure 6. Normal probability plot of the standardized effects for (A) piezoelectric coefficient (B) dielectric permittivity (C) relative density (D) dimensional accuracy.

Crystal structure of the samples was analyzed by x-ray diffraction (XRD) on a D8 discover diffractometer (Brucker). Figure 5 shows the XRD for 100 nm and 300 nm BaTiO<sub>3</sub> particle size after sintering using a range  $2\theta$  from 20° to 80°. The peaks splitting at (002) and (200) for both particle size index for a tetragonal crystal structure [37, 38]. Previous studies report that a transition from cubic to tetragonal phase can be observed in BaTiO<sub>3</sub> using heat treatments above 1000 °C [39–41]. A higher intensity of (002) and (200) peaks was observed for the 100 nm BaTiO<sub>3</sub> sample, which can be attributed to a higher amount of crystals in the tetragonal phase. Researchers reported that the growth of BaTiO<sub>3</sub> crystallite strongly depend on the heat temperature and exposure time during the sintering process [40].

#### 3. Statistical results

This study considered the piezoelectric coefficient, dielectric permittivity, density, and dimensional accuracy as critical outputs to fabricate BaTiO $_3$  ferroelectric ceramics. All the experimental results were collected (supplementary sections 4–7, tables 4–7) and analyzed in Minitab. The normal probability plots of the standardized effect provided in figure 6 presents the factors that have a statistical significance with respect to every individual output at a 95% confidence level. The interaction plot (supplementary section, figures 11–13; figure 7) evaluates the effect of two variables and their impact on the end-output at a 95% confidence level. The interaction plot is significant when the effect of a factor with a specific output depends on another factor [42]. Lastly, the main effect plots shown in figure 8 presents an analysis of factors and levels that maximize every output.

For the piezoelectric response shown in figure 6(A) the only significant factor was the BaTiO<sub>3</sub> particle size. Figure 8(A) indicates that the 100 nm particle size is the level that will maximize the piezoelectric coefficient of the samples. This result is a good agreement with literature, which indicates that an increase on piezoelectric properties is observed when decreasing particle size of BaTiO<sub>3</sub> [36, 37]. Figure 6(B) indicates that the factors affecting the dielectric permittivity were the PVA concentration and the interaction (figure 7) of PVA and BaTiO<sub>3</sub>. Figure 8(B) shows that 13% PVA is the level that will increase the dielectric permittivity. Results in the interaction plot indicate that the combination of PVA and BaTiO<sub>3</sub> that maximize the output is 100 nm BaTiO<sub>3</sub> and 13% PVA concentration. PVA is a carbon base binder, and although PVA was burnout during sintering, literature indicates that carbon residues may be encapsulated affecting the permittivity of ceramics [38, 43]. Figure 6(C) shows that the only significant factor that has an impact on the density was the BaTiO<sub>3</sub> particle size.

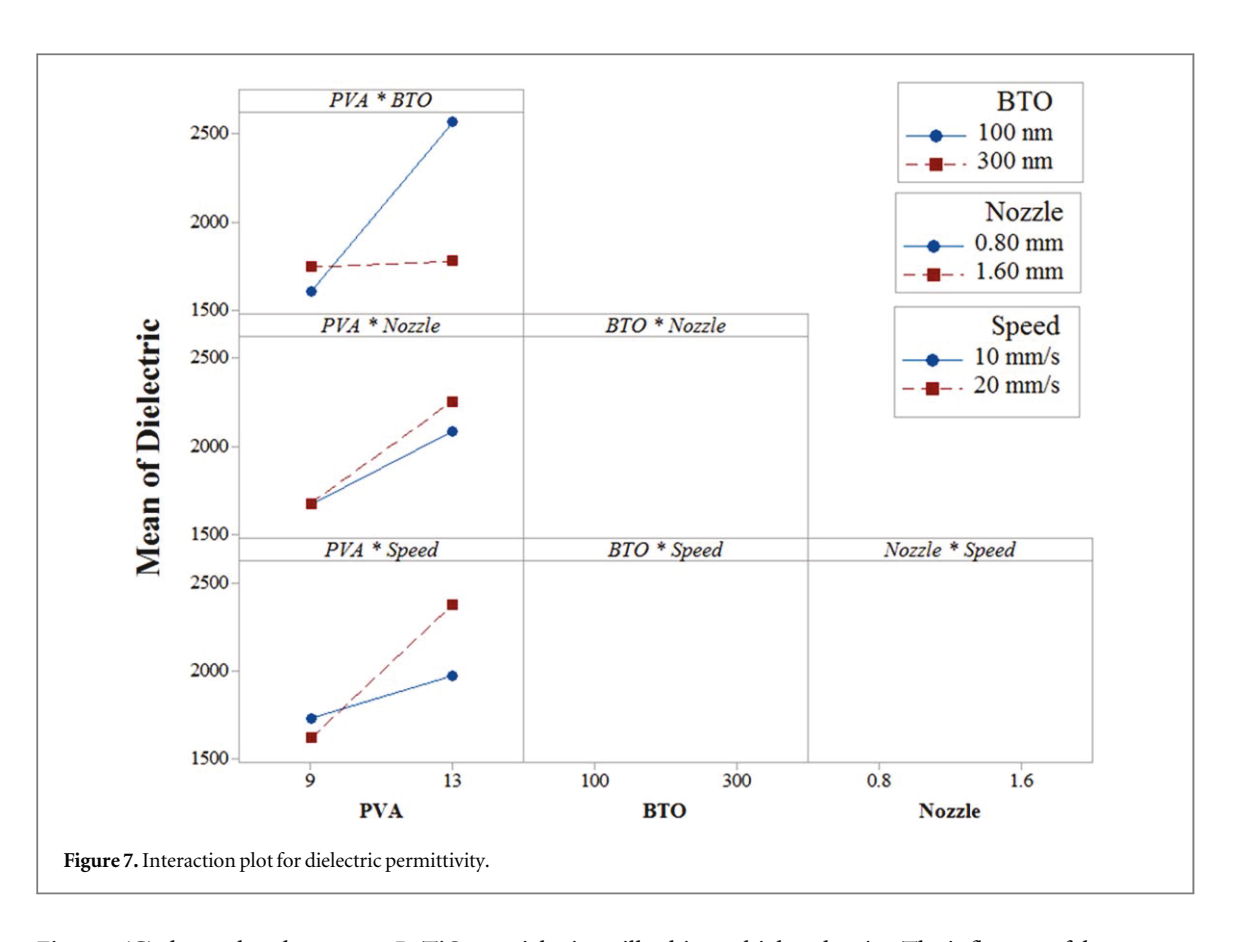
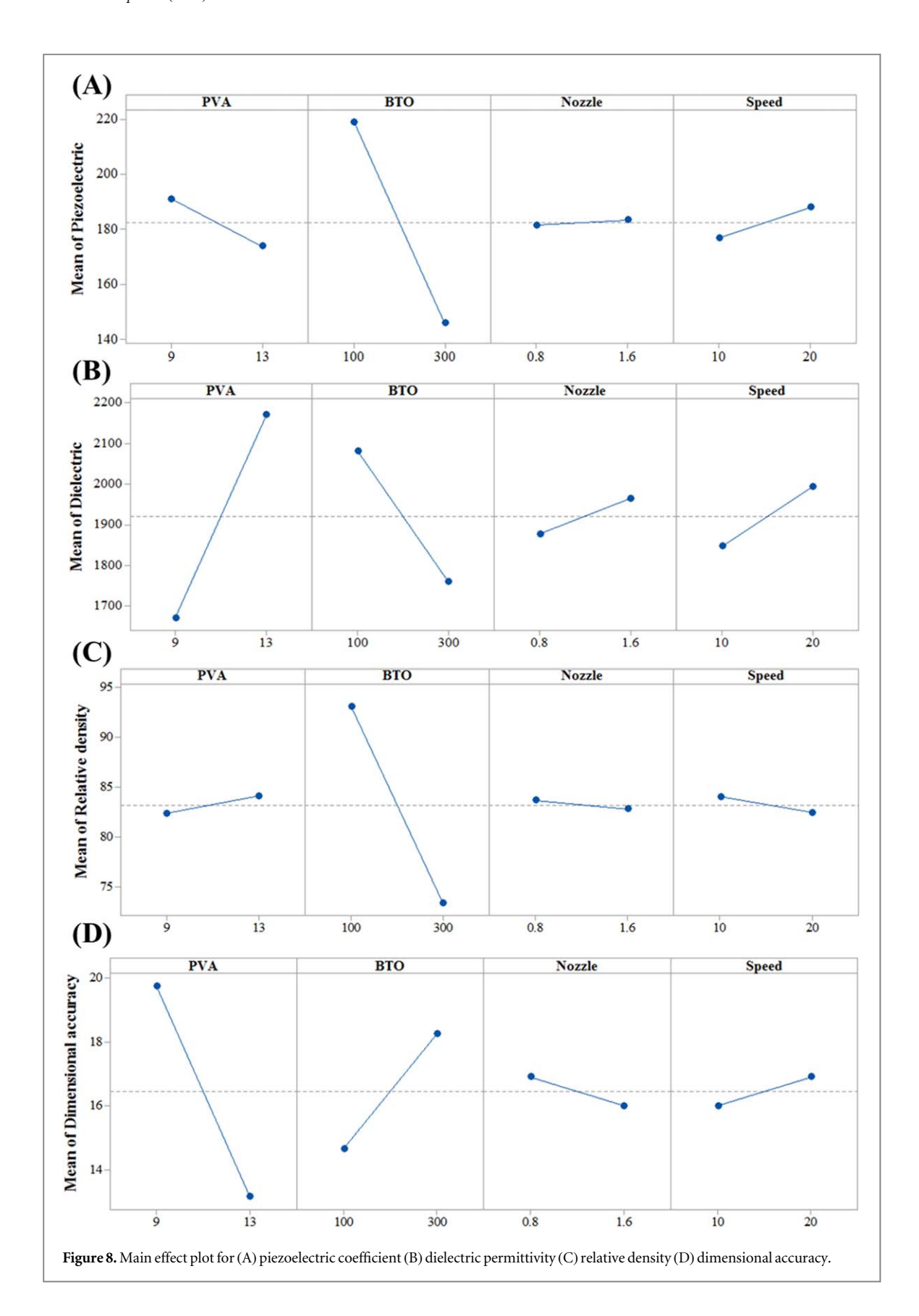


Figure 8(C) shows that the  $100 \text{ nm BaTiO}_3$  particle size will achieve a higher density. The influence of the ceramic particle size is consistent with previous studies [35] suggesting that finer particle size normally achieve a higher grain growth due to high curvature of the powder. For dimensional accuracy, it was found that the PVA concentration was the only significant factor as shown in figure 6(D). Figure 8(D) indicates that 13% PVA is the level that minimizes the angle of deformation and enables a better stack of material. This result is in good agreement with the rheology of the paste (figures 1–2), which indicates that there is an increase in viscosity for higher binder contents.

Based on the results obtained in the factorial  $2^{k-1}$  design, it was found that the parameters that positively affect the end-outputs are 100 nm BaTiO<sub>3</sub> and 13% PVA concentration. There is no evidence to claim that the printing speed and the nozzle diameter affects the output evaluated in this study. Therefore, to optimize the fabrication of BaTiO<sub>3</sub> ferroelectric ceramics, the printing speed and nozzle diameter can be neglected and use either level of said factors. From the experimental results, a predictive probability model can be created by minimizing the uncertainty on the estimated effect for different design points [42]. The probability cube plot (supplementary section 9, figures 14–17) considered a fitted means analysis, which is useful to predict the outputs in a balanced design [26]. The fitted means analysis indicates that 100 nm BaTiO<sub>3</sub> and 13% PVA concentration enables the fabrication of ferroelectric ceramics with a piezoelectric coefficient higher than 200 pC/N. While the 300 nm BaTiO<sub>3</sub> can achieve a piezoelectric coefficient of only 135 pC/N. The mean predicted piezoelectric coefficient represents 48% higher value compared to any other combination levels analyzed in this study. Dielectric permittivity is predicted to be higher than 2200. Additionally, using the optimal interaction levels from the probability cube for PVA and BaTiO<sub>3</sub> makes it possible to achieve 33% higher permittivity. The density is predicted to be about 90% with respect to the theoretical value of pure BaTiO<sub>3</sub>, which is 33% higher than any other combination of levels. Additionally, a low angle of deformation of about 10 degrees can be achieved, representing a 44% increase in dimensional accuracy. These predicted outputs are comparable with the BaTiO<sub>3</sub> theoretical values, proving its capabilities to use FEF 3D printing technique for the fabrication of complex geometries for commercial applications.

#### 4. Conclusion

A DOE for BaTiO<sub>3</sub> ferroelectric ceramics using FEF 3D printing technique was presented. This paper aimed to optimize the formulation of the ceramics suspensions to produced defects-free samples. This study considered the evaluation of BaTiO<sub>3</sub> particle size, PVA concentration, printing speed, and nozzle diameter. Results showed



that the  $BaTiO_3$  particle size positively affects the piezoelectric coefficient, dielectric permittivity and density of the samples. In another hand, it was found that the PVA concentration has an impact on dielectric permittivity and dimensional accuracy. The optimal levels are 100 nm for  $BaTiO_3$  and 13% PVA concentration. The printing speed and nozzle diameter do not influence the desired end-product outputs. Using the optimal levels in the paste formulation, it is possible to fabricate samples with 90% density. A piezoelectric coefficient higher than

200 pC/N and a dielectric permittivity higher than 2200 can be obtained. Additionally, a low angle of deformation of about 10 degrees can be achieved, which is a good parameter for dimensional accuracy. These results correspond to the full theoretical properties normally achieve by traditional manufacturing techniques for BaTiO<sub>3</sub> ceramics. Therefore, this paste extrusion technique can be used in the fabrication of more complex geometries and extend the applications of piezoelectric ceramics for sensors and actuators with designed geometry.

#### Acknowledgments

This research is funded by the Department of Energy (DOE) under Grant No. DE-FE0027502, and DE-NA0003865.

#### **ORCID** iDs

Anabel Renteria https://orcid.org/0000-0001-9013-8115 Luis A Chavez https://orcid.org/0000-0001-5203-6708 Yingtao Liu https://orcid.org/0000-0002-6232-9704

#### References

- [1] Conner B P, Manogharan G P, Martof A N, Rodomsky L M, Rodomsky C M, Jordan D C and Limperos J W 2014 Making sense of 3D printing: creating a map of additive manufacturing products and services *Additive Manufacturing* 1–4 64–76
- [2] Deckers J, Vleugels J and Kruth J-P 2014 Additive manufacturing of ceramics: a review *Journal of Ceramic Science and Technology* 5
- [3] Mason M S, Huang T, Landers R G, Leu M C and Hilmas G E 2009 Aqueous-based extrusion of high solids loading ceramic pastes: process modeling and control *J. Mater. Process. Technol.* 209 2946–57
- [4] Pal D, Chakraborty A K, Sen S and Sen S K 1996 The synthesis, characterization and sintering of sol-gel derived cordierite ceramics for electronic applications *J. Mater. Sci.* 31 3995–4005
- [5] Ogihara H, Randall C A and Trolier-Mckinstry S 2009 High-energy density capacitors utilizing 0.7BaTiO<sub>3</sub>-0.3 BiScO<sub>3</sub> ceramics *J. Am. Ceram. Soc.* 92 1719–24
- [6] Eckel Z C, Zhou C, Martin J, Jacobsen A J, Carter W B and Schaedler T A 2016 Additive manufacturing of polymer-derived ceramics Science, Rep. 351 58–62
- [7] Peng E, Zhang D and Ding J 2018 Ceramic robocasting: recent achievements, potential, and future developments Adv. Mater. 30 1802404
- [8] Huang T, Mason M S, Zhao X, Hilmas G E and Leu M C 2009 Aqueous-based freeze-form extrusion fabrication of alumina components *Rapid Prototyping Journal* 15 88–95
- [9] Huang T, Mason MS, Hilmas GE and Leu MC 2006 Freeze-form extrusion fabrication of ceramic parts *Virtual and Physical Prototyping* 193–100
- [10] Smay J, Gratson G, Shepherd R, Cesarano J and Lewis J 2002 Directed colloidal assembly of 3D periodic structures Adv. Mater. 14
- [11] Zhao S, Xiao W, Rahaman M N, Obrien D, Seitz-Sampson J W and Bal B S 2016 Robocasting of silicon nitride with controllable shape and architecture for biomedical applications *Int. J. Appl. Ceram. Technol.* 14 117–27
- [12] Kim H, Renteria-Marquez A, Islam M D, Chavez L A, Rosales C A G, Ahsan M A, Tseng T-L B, Love N D and Lin Y 2018 Fabrication of bulk piezoelectric and dielectric BaTiO<sub>3</sub> ceramics using paste extrusion 3D printing technique *J. Am. Ceram. Soc.* 102 3685–3694
- [13] Ding C, Liu L, Mei Y, Ngo K D T and Lu G-Q 2018 Magnetic paste as feedstock for additive manufacturing of power magnetics 2018 IEEE Applied Power Electronics Conf. and Exposition (APEC)
- [14] Eerenstein W, Mathur ND and Scott JF 2006 Multiferroic and magnetoelectric materials Nature 442 759-65
- [15] Jaffe B, Cook W R and Jaffe H 1971 The piezoelectric effect in ceramics *Piezoelectric Ceramics* (New York: Academic Press Inc) 7–210-
- [16] Liu W and Ren X 2009 Large piezoelectric effect in Pb-free ceramics Phys. Rev. Lett. 103 257602
- [17] Renteria-Marquez I, Renteria-Marquez A and Tseng B 2018 A novel contact model of piezoelectric traveling wave rotary ultrasonic motors with the finite volume method *Ultrasonics* 90 5–17
- [18] Karaki T, Yan K, Miyamoto T and Adachi M 2007 Lead-free piezoelectric ceramics with large dielectric and piezoelectric constants manufactured from BaTiO<sub>3</sub> nano-powder *Japan. J. Appl. Phys.* 46 4–7
- [19] Wu J, Xiao D and Zhu J 2015 Potassium–sodium niobate lead-free piezoelectric materials: past, present, and future of phase boundaries Chem. Rev. 115 2559–95
- [20] Zheng T, Wu J, Xiao D and Zhu J 2018 Recent development in lead-free perovskite piezoelectric bulk materials Prog. Mater Sci. 98 552–624
- [21] Shrout T R and Zhang S 2007 Lead-free piezoelectric ceramics: alternatives for PZT? J. Electroceram. 19 185–185
- [22] Chen H and Zhao Y F 2016 Process parameters optimization for improving surface quality and manufacturing accuracy of binder jetting additive manufacturing process Rapid Prototyping Journal 22 527–38
- [23] Wang Y and Zhao Y F 2017 Investigation of sintering shrinkage in binder jetting additive manufacturing process Procedia Manufacturing 10 779–90
- [24] Shrestha S and Manogharan G 2017 Optimization of binder jetting using Taguchi method JOM 69 491–7
- [25] Yan C, Li S, Yang L and He L 2018 Investigation of FEF process liquid phase migration using orthogonal design of experiments Rapid Prototyping Journal 25 388–396
- [26] Montgomery D C 2017 Design and Analysis of Experiments (New York: Wiley) pp 320–93

- [27] Yong-An H, Biao L, Yi-Xuan Z, Dan-Dan L, Ying-Bang Y, Tao T, Bo L and Sheng-Guo L 2018 Grain size effect on dielectric, piezoelectric and ferroelectric property of BaTiO<sub>3</sub> ceramics with fine grains *Journal of Inorganic Materials* 33 767
- [28] Rowe G M, King G and Anderson M 2014 The influence of binder rheology on the cracking of asphalt mixes in airport and highway projects *J. Test. Eval.* 42 20130245
- [29] M'Barki A, Bocquet L and Stevenson A 2017 Linking rheology and printability for dense and strong ceramics by direct ink writing Sci. Rep. 7 6017
- [30] Gao H-W, Yang R-J, He J-Y and Yang L 2009 Rheological behaviors of PVA/H<sub>2</sub>O solutions of high-polymer concentration J. Appl. Polym. Sci. 116 1459–1466
- [31] Do T-A, Hargreaves J, Wolf B, Hort J and Mitchell J 2007 Impact of particle size distribution on rheological and textural properties of chocolate models with reduced fat content *J. Food Sci.* 72 E541–E552
- [32] Quemada D 1978 Rheology of concentrated disperse systems II. A model for non-newtonian shear viscosity in steady flows *Rheol. Acta* 17 632–42
- [33] Misra R 2002 Controlled drying to enhance properties of technical ceramics Chem. Eng. J. 86 111-6
- [34] Mason W P and Matthias B T 1948 Theoretical model for explaining the ferroelectric effect in barium titanate Phys. Rev. 74 1622–36
- [35] Novak N, Pirc R and Kutnjak Z 2014 Effect of electric field on ferroelectric phase transition in BaTiO<sub>3</sub> ferroelectric Ferroelectrics 469
- [36] Ting J M and Lin R Y 1995 Effect of particle size distribution on sintering J. Mater. Sci. 30 2382–9
- [37] Cullity B D and Stock S R 2015 Elements of x-ray diffraction (India: Pearson Education) Miejsce nieznane 9789332535169
- [38] Frey M H and Payne D A 1996 Grain-size effect on structure and phase transformations for barium titanate Phys. Rev. B 54 3158-68
- [39] Schumacher B, Gebwein H, Hanemann T and Haubelt J 2008 Influence of the crystallite BaTiO<sub>3</sub> on dielectric properties of polyester reactive resin composite materials Tech. Connect Briefs 1 385–8
- [40] Elqudsy M A, Widodo R D, Rusiyanto R and Sumbodo W 2017 The particle and crystallite size analysis of BaTiO3 produced by conventional solid-state reaction process AIP Conf Proc 1818
- [41] Hoshina T, Hatta S, Takeda H and Tsurumi T 2018 Grain size effect on piezoelectric properties of BaTiO<sub>3</sub> ceramics Japan. J. Appl. Phys.
- [42] Uy M and Telford J K 2009 Optimization by design of experiment techniques 2009 IEEE Aerospace Conf.
- [43] Robinson S K and Paul M R 2001 Debinding and sintering solutions for metals and ceramics Met. Powder Rep. 56 24-34